Article

JFPE

Journal of Fire Protection Engineering
21(2) 141–166

DOI: 10.1177/1042391510388879
jfe.sagepub.com

SAGE

Analyzing smoke alarm response to flaming fires using the fire model JET

William Davis, Nathan Marsh and Michael Selepak
National Institute of Standards and Technology, Gaithersburg, MD, USA

Abstract
An algorithm that calculates the time dependent smoke concentration in a fire-induced ceiling jet within a smoke layer and algorithms for predicting the response of photoelectric smoke alarms, both of which are part of the computer model JET, are examined using three different fires in a small room. The objectives of this analysis are to test the ceiling jet smoke algorithm and understand the limitations of analyzing signals from photoelectric smoke alarms located in the ceiling jet to estimate fire size and thereby support decision making by emergency responders. The analysis is restricted to flaming fires that produce turbulent plumes and can be represented by axisymmetric point sources. Two different smoke yields from the literature are used to obtain ceiling jet smoke density from JET. Depending on the value of the smoke yield used, the predictions of JET follow or do not follow the photoelectric smoke alarm signals. This suggests that additional information about how smoke yields are measured or that a better calibration technique is required in order to accurately model smoke alarm response.

Keywords
Ceiling jet, computer model, fire detection, fire experiments, photoelectric smoke alarms, smoke algorithm

Introduction

The signals output by photoelectric smoke alarms should be useful in sensing and measuring the development of a growing fire. This article investigates that

Corresponding author:
William Davis, National Institute of Standards and Technology, 100 Bureau Drive, Gaithersburg, MD 20899, USA
Email: william.davis@nist.gov

possibility by testing a ceiling jet algorithm designed to predict smoke concentration in the ceiling jet. Predicting the signal output by a photoelectric smoke alarm in response to a growing fire requires calculating the time dependent evolution of the smoke concentration in the ceiling jet. Some of the early efforts focused on just smoke alarm activation and used the temperature rather than the smoke concentration to predict smoke detector activation due to the availability of correlations that gave ceiling jet temperature [1] and the assumption that smoke concentration can be related to ceiling jet temperature [2,3]. Using temperature to predict smoke detector activation ignores differences in the way that different detectors react to the production of smoke by burning materials that may completely invalidate a temperature/smoke prediction correlation. Overviews of issues associated with modeling smoke detection can be found in Schifiliti's [4] article and in an article by Bukowski and Averill [5]. A study of the performance of several types of alarms in a residential setting can be found in [6].

There have been efforts to use computational fluid dynamics (CFD) to calculate the smoke concentration in the ceiling jet and with the increased computer power available today, these methods are becoming practical [7,8]. However, there is still a need for an algebraic correlation that would yield smoke concentration in the ceiling jet and not require substantial computer power and computer time to obtain the solution. Early work on the ceiling jet resulted in successful unconfined ceiling jet temperature and velocity correlations [9] that are in use today. Later, Yamauchi [10] extended this work to calculate the smoke concentration and smoke alarm activation in the ceiling jet when a hot layer was developing. Yamauchi's method required the solution of a set of differential equations in order to define the ceiling jet properties as well as a zone model to define the depth and temperature of the hot layer.

In this article, the predictions of an algorithm used to calculate the smoke concentration in the ceiling jet in the presence of a smoke layer and algorithms for predicting the response of photoelectric smoke alarms that are part of the computer model JET [11] will be examined using three different fires in a small room. The analysis will be restricted to flaming fires that produce turbulent plumes, which can be represented by axisymmetric point sources. The output from photoelectric smoke alarms as well as a laser will be used to determine smoke density in the ceiling jet. The signals from these devices will be converted to light extinction coefficients and compared with the predictions of JET.

JET is a single compartment zone model that calculates the temperature, smoke and gas concentration in the plume, ceiling jet, and upper layer. The lower layer is assumed to remain at ambient conditions. JET has been compared against a number of experiments to measure the predictive capability of its algorithms for ceiling jet temperature, layer temperature, heat detector activation, and sprinkler activation [11]. This article represents an effort to examine the capabilities of the smoke algorithm in JET.

Ceiling jet algorithm

The algorithm used in the computer model JET for calculating the smoke or carbon monoxide concentration in the plume and ceiling jet (scalar concentration) has been described in detail by Davis et al. [12]. Only the final equations will be presented here in order to provide the theoretical foundation to discuss the results. The following assumptions were made in order to simplify the equations used to derive the algorithm. The fire is represented by a point source and assumed to be axisymmetric. The zone model approximation of homogeneous temperature and particle densities in each layer is assumed. Gaussian shapes in the radial direction will represent the velocity, temperature, smoke density, and combustion gas profiles in the plume. All air entrained into the plume below the smoke layer interface will be considered to be smoke free. Agglomeration and coagulation effects, particle inertia and diffusion effects, and smoke deposition on the walls are not included in the algorithm. In the following description, the term scalar concentration will be used rather than smoke concentration as the algorithm is applicable to both smoke and gas products from the fire. The equation set given below replaces the fire source and two-layer environment with a substitute fire source and a single-layer environment. At the layer interface, it is required that the scalar concentration be continuous and that the scalar mass flux be conserved.

With a smoke layer present and with the fire source below the smoke layer, the maximum scalar mass concentration $C_{sm}(r)$ at a radial distance from the plume centerline in the ceiling jet of $r > r_e$ (Ref. [9]) is given by:

$$C_{sm}(r) = \frac{\sqrt{2}\left(\frac{\lambda^2}{\lambda^2+1}\right) D \dot{Q}_2^{*2/3} \left(\frac{Z_2}{H_2}\right)^{5/3} \left(\frac{r_e}{r}\right)^{0.57}}{\left(1 + k \dot{Q}_2^{*2/3} \left(\frac{Z_2}{H_2}\right)^{5/3}\right)} + C_L. \tag{1}$$

where

$$D = \frac{Y_s \left(\frac{\lambda^2+1}{\lambda^2}\right) \rho_\infty C_P T_\infty}{15.4 H_c (1-\chi_r)^{1/3} C_l^2}, \tag{2}$$

$$\dot{Q}_1^* = \frac{\dot{Q}}{\rho_\infty C_p T_\infty g^2 Z_1^{5/2}}, \tag{3}$$

$$\dot{Q}_2^* = \left[\frac{D \dot{Q}_1^{*2/3} - C_L\left(1 + k \dot{Q}_1^{*2/3}\right)}{D + C_L k \left(1 + k \dot{Q}_1^{*2/3}\right)}\right]^{3/2}, \tag{4}$$

$$Z_2 = Z_1 \left[\frac{\dot{Q}_1^*}{\left(\dot{Q}_2^* + \frac{(\lambda^2+1)}{\lambda^2} \frac{C_L}{D} \left(1 + k \dot{Q}_2^{*2/3} \right) \dot{Q}_2^{*1/3} \right)} \right]^{2/5}, \tag{5}$$

$$H_2 - Z_2 = H_1 - Z_1, \tag{6}$$

$$k = 9.1(1 - \chi_r)^{2/3}, \tag{7}$$

$$Z_1 = z - zo, \tag{8}$$

$$z_0 = -1.02d + 0.083 \dot{Q}^{2/5}, \tag{9}$$

where C_1 is 0.12, C_L the scalar mass concentration in the layer ($g\,m^{-3}$), C_p the heat capacity of the gas at constant pressure ($kJ\,(kg\,K)^{-1}$), d the fire diameter (m), g the acceleration of gravity ($m\,s^{-2}$), H_1 the ceiling height from the fire surface (m), H_2 the ceiling height from the origin of the substitute source (m), H_c the chemical heat of combustion for each fuel ($kJ\,g^{-1}$), k the constants associated with the plume centerline temperature equation, $\dot{Q}$ the heat release rate (HRR) of the fire (kW), r the radial distance from the plume centerline (m), r_e the 0.18 H_1 (m) T_∞ the ambient temperature (K), $\underline{Y}_s$ the product yield fraction for each fuel, z the height to the layer interface from fuel surface (m), Z_1 the height to the layer interface from the virtual origin (m), Z_2 the height to the layer interface from the origin of the substitute source (m), z_0 the height of virtual origin above fuel surface (m), λ^2 is 1.157, which is the square of the ratio of the 1/e width of the plume scalar profile to the plume velocity profile, ρ_∞ the ambient gas density ($kg\,m^{-3}$), χ_r the radiative fraction, and 1, 2 the subscripts for source and substitute source variables.

With the appropriate product-yield fraction, heat of combustion, and radiative fraction in Equation (2), Equation (1) predicts the concentration of smoke, CO, or other combustion product in the ceiling jet.

The alarm algorithms for smoke and gas in the zone model JET take the form of either a single differential equation (Equation (10)) or two differential equations (Equations (10) and (11)). Modeling smoke density inside a smoke alarm typically requires only a single differential equation while CO density inside a CO detector is best represented by both equations [12,13]. The general equation set used to represent the two-step diffusion process for the alarms is:

$$\frac{dX(t)}{dt} = [X_e(t - \delta\tau) - X(t)]/\tau. \tag{10}$$

$$\frac{dX_s(t)}{dt} = [X(t) - X_s(t)]/\tau. \tag{11}$$

$$\delta\tau = au_e^{-c}. \tag{12}$$

$$\tau = bu_e^{-d}. \tag{13}$$

$X(t)$ is the smoke or gas mass density in the sensing chamber, X_e the smoke or gas mass density at the location of the alarm, X_s the gas mass density at the electrochemical sensor, u_e the flow velocity outside of the detector housing, $\delta\tau$ the lag or offset time for the flow to travel through the detector to the sensing chamber, τ the mixing time in the sensing chamber, and a, b, c, and d determined from the response time fits of the alarm. For flow velocities above $0.1\,\mathrm{m\,s^{-1}}$, $\delta\tau$ and τ become less sensitive to velocity variations for the alarms tested and can be treated as constants, which was the case for the experiments considered here. For the photoelectric smoke detectors analyzed, a lag time of 2 s and a mixing time of 0.2 s were used based on measurements using the fire emulator/detector evaluator (FE/DE) [14] and analysis of the current data set.

The extinction coefficient per unit mass, $(8.7 \pm 1.1)\,\mathrm{m^2\,g^{-1}}$ (Ref. [15]) at 633 nm for flame generated smoke is used to convert the scalar (smoke) density ($\mathrm{g\,m^{-3}}$) to the extinction coefficient K for over-ventilated flaming fires. While many smoke alarms use lasers with wavelengths in the near-infrared, the 633 nm wavelength was chosen to be consistent with the calibration laser used with the FE/DE [14] and the laser used in the experiment. The factor $8.7\,\mathrm{m^2\,g^{-1}}$ is based on measurements at 633 nm. The wavelength dependence of this factor must be accounted for in order to convert smoke density to extinction when using laser systems operating at different wavelengths [16].

The defining equation for the extinction coefficient in a homogeneous medium is:

$$\frac{I_\lambda}{I_{\lambda 0}} = e^{-KL}. \tag{14}$$

where I_λ is the final intensity at wavelength λ, $I_{\lambda 0}$ the incident intensity, L the path length, and K the extinction coefficient at that wavelength.

Modeling fires with JET

JET is a two-layer zone model where the conservation equations for mass and energy determine the upper or smoke layer development and the lower layer is assumed to stay at ambient temperature with no mixing of smoke into the lower layer. The room pressure is assumed to remain constant. These assumptions will cause JET to under-predict temperatures and smoke concentrations in spaces with large fires where the fire size is sufficient to heat the lower layer or cause the lower

layer to become smoky as JET will calculate the lower-layer entrainment based on ambient conditions.

JET is designed to be used for spaces that are partitioned by draft curtains or for rooms where the only opening is a door or several doors of equivalent height and the draft curtain option can be used to represent room walls. For the experiments described in this article, the room walls were represented by a draft curtain that extended to 0.30 m above the floor and was equal in length to the perimeter of the room. The draft curtain does not absorb heat.

When modeling detection devices such as smoke alarms that can alarm early in the development of a fire, a layer delay time is used to represent the fact that the formation of the upper layer does not occur until the ceiling jet flow has had a chance to reflect off the walls of the enclosure and flow back toward the plume. Once this return flow reaches the plume, it will start supplying smoke to the plume and increase the smoke concentration in the plume and ceiling jet. This return flow is what forms the upper layer. The substitute source method is used to derive the ceiling jet algorithm in JET that approximates this behavior. Failure to include a layer delay time will cause JET to under-predict the time to alarm.

JET calculates the maximum temperature and maximum scalar concentration in the plume at the ceiling and in the ceiling jet as a function of distance from the plume centerline. The model does not provide a temperature profile or scalar concentration profile beneath the ceiling. JET can also calculate the average upper layer temperature and scalar concentration, ceiling temperature profile, impact of forced ventilation on the upper layer, and heat, smoke, CO, and sprinkler activation.

In order to model the experiments discussed in this article using the computer model JET, the following user inputs are required:

- Length, width, and height of room.
- Curtain length and height.
- Ceiling properties including thermal conductivity, heat capacity, density, and thickness.
- Ambient temperature.
- Height to the top of the fuel source measured from the floor.
- Fire diameter (constant or as a function of HRR).
- HRR and radiative fraction as a function of time.
- Heat of combustion and smoke yield of the fuel.
- Radial distance of each detector from the fire centerline.
- Detector type, number of equations to model detector, and offset or entry time.
- Layer delay time (based on room size and estimated ceiling jet flow speeds).
- Output time interval and computation end time.

To use JET to predict smoke alarm activation, use the smoke concentration predicted by JET for the sensing chamber of the alarm and the appropriate wavelength dependent conversion factor to convert the smoke density to extinction. When the alarm extinction level is reached, the alarm should sound.

Gas alarms are treated in a similar fashion except when the concentration in the sensing chamber reaches the target concentration, the alarm should sound. If JET is used to predict activation, a correction must be included for the smoke travel time to the alarm. The experiments performed here examined how well the smoke algorithm in JET could track a photoelectric smoke alarm output at smoke concentrations above the typical photoelectric smoke alarm set point and were not designed to test activation predictions.

Experiments

Experiments were conducted to test the capability of the ceiling jet algorithm in JET to predict smoke density in the ceiling jet from smoke produced by flaming fires. The experiments were conducted in a room with floor dimensions of 3.16×3.05 m with a floor to ceiling height of 2.46 m. Small amounts of heptane (50 mL) or toluene (10 mL), placed in a small dish of diameter 89 mm or a block of black polymethyl-methacrylate (PMMA) ($0.076 \times 0.076 \times 0.0127$ m) were used as fuels and were placed on a load cell that was centered in the room. The distance from the floor to the top of the dish was 0.127 m. The heat release rate (HRR) was obtained by measuring the mass loss rate and multiplying by the chemical heat of combustion of the fuel (Table 1). For these small fires, the HRR was not oxygen limited. The flat, smooth ceiling was made up of acoustic ceiling tile. The walls of the room were constructed of glazed cinderblocks except for one that was constructed of ceiling tile. The door to the room was closed during the experiment.

Instrumentation included 17 thermocouples, a velocity probe, an air-cooled diode laser extinction meter to measure extinction coefficients, and five commercial photoelectric smoke alarms. Temperature measurements in the ceiling jet were conducted using type *K* bare bead (0.76 mm diameter) thermocouples positioned 0.01 m below the ceiling at radial positions shown in Figure 1. A thermocouple tree (TT) located 0.60 m from plume center with thermocouples located vertically below

Table 1. Heat of combustion, radiative fraction, and smoke yield.

Fuel	Chemical heat of combustion, ΔH_c (KJ g^{-1})	Radiative fraction, χ_r	Smoke yield, Y_s
Propene (C_3H_6)	40.5[17]	0.37[17]	0.095[17]
Heptane	41.2[17]	0.33[17]	0.0129[18]
(C_7H_{16})			0.037[17]
Toluene (C_7H_8)	27.7[17]	0.60[17]	0.100[18]
		0.31–0.37[19,20]	0.178[17]
PMMA ($C_5H_8O_2$)	24.2[17]	0.314[17]	0.022[17]

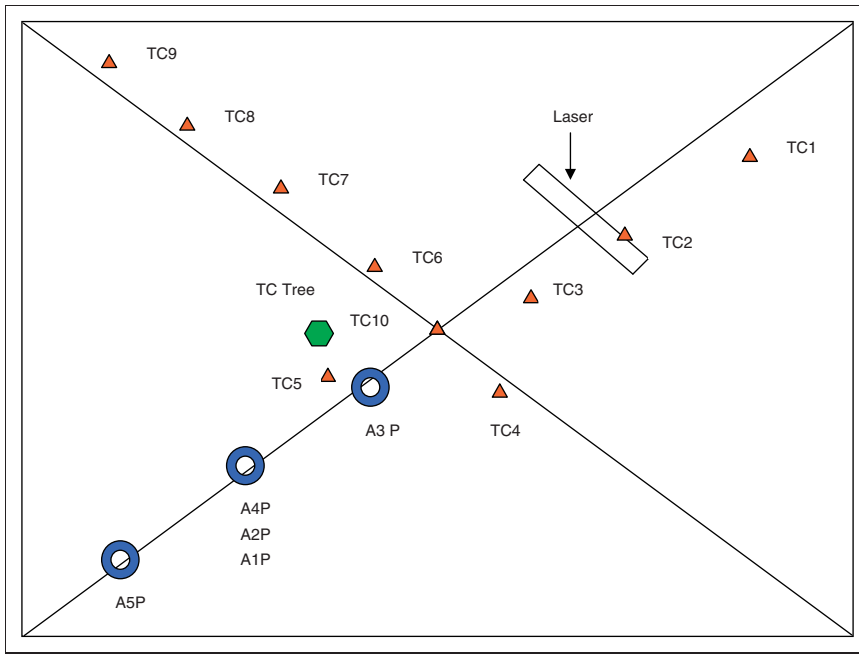

Figure 1. Layout of instrumentation in the test room.
Notes: Triangles ▲ are thermocouples (TC), donuts ◎ are photoelectric smoke alarms (P) hexagon ⬢ is a TT and the rectangle ▭ is a laser/diode detector. Distances are measured radially from the center of the fire source where TC10 is located.

the ceiling at 0.01, 0.03, 0.06, 0.12, 0.24, 0.36, and 0.50 m were used to measure the depth of the ceiling jet and the temperature in the smoke layer. The voltage output of the photoelectric smoke alarms was compared with the extinction coefficient measurement using a diode laser operating at 630 nm. The calibration fire source was a propene burner that was chosen for its smoke output and was operated at a series of fire sizes. The calibration curve fit equations and a sample curve fit for the smoke alarms are found in the Appendix. The calibration fits covered an extinction coefficient range from approximately 0.05 to 0.25 m^{-1}. The fits were linear which permitted extrapolation outside the measurement range although this type of extrapolation can lead to errors if the output of the photoelectric smoke alarm deviates from the extrapolation values. Since these experiments had simultaneous laser extinction and photoelectric smoke alarm measurements, extrapolation errors would be expected only if the photoelectric smoke alarm measurements deviated from the laser measurements.

The smoke extinction laser was mounted such that the exposed laser beam was located radially 1.0 m from the plume centerline, 0.038 m beneath the ceiling and had a path length of 0.5 m. The laser wavelength was 630 nm. The diode detector was also air-cooled. The photoelectric smoke alarm entry ports were located

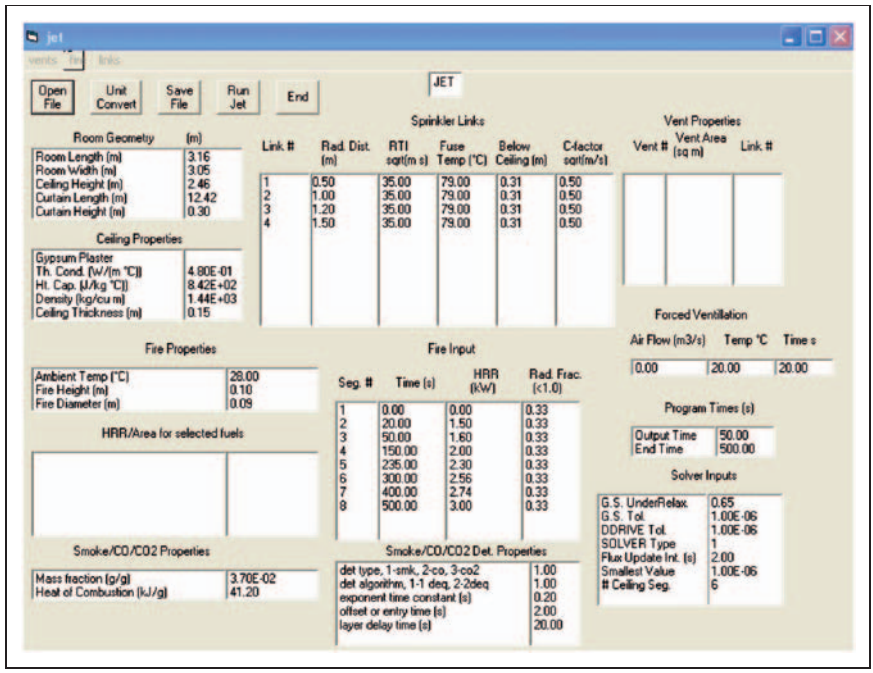

Figure 2. Example input file used to model heptane.

0.025 m beneath the ceiling. Figure 1 shows the locations of the photoelectric smoke alarms and the laser. By measuring the decrease in intensity of the laser or the changing voltage of the alarms, the extinction coefficient could be determined.

Values for the heat of combustion, radiation fraction, and smoke yield for the fuels used in the experiments, heptane, toluene, and PMMA, were obtained from a publication by Tewarson [17] except for two smoke yields that were obtained from a publication by Mulholland [18] and are tabulated in Table 1. Toluene presents an additional modeling challenge as the radiative fraction has multiple values reported in the literature [17,19,20].

The load cell used to measure the mass loss of the fuels was calibrated using a standard weight set and was found to be accurate to 0.01 g. For very small mass losses, the load cell vibration produced by the fire was averaged out; only for the smallest mass loss measured (0.005 g) was this an issue.

Temperature measurements are reported as excess temperature. Excess temperature is defined as the difference between the measured temperature and ambient temperature. Signals from the thermocouples, laser, alarms, and load cell were sampled every second.

Figures 2–4 provide examples of the inputs used for JET in modeling the heptane, PMMA, and toluene experiments. A number of calculations with different input values for χ_r and Y_s were used to model heptane and toluene in order to

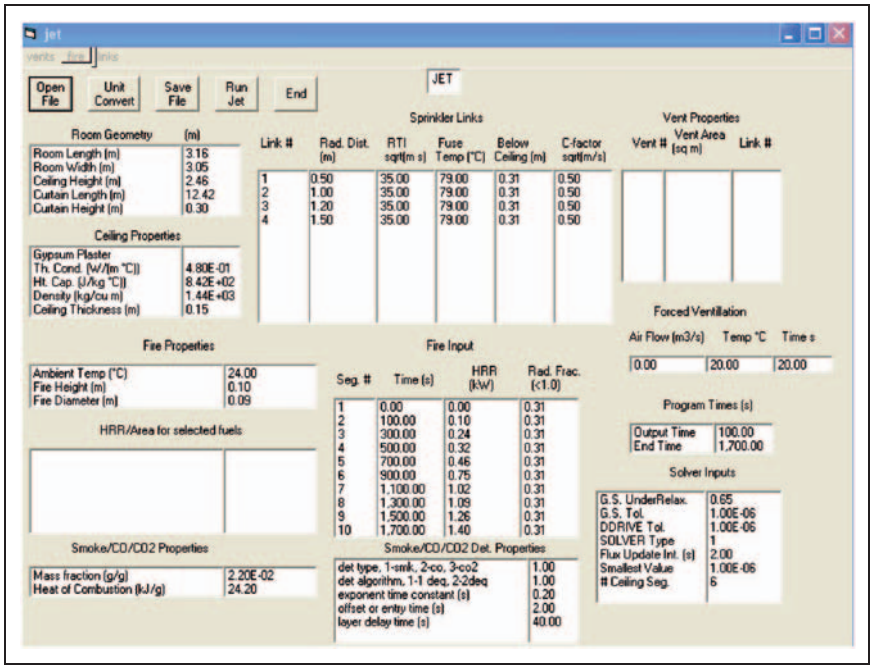

Figure 3. Example input file used to model PMMA.

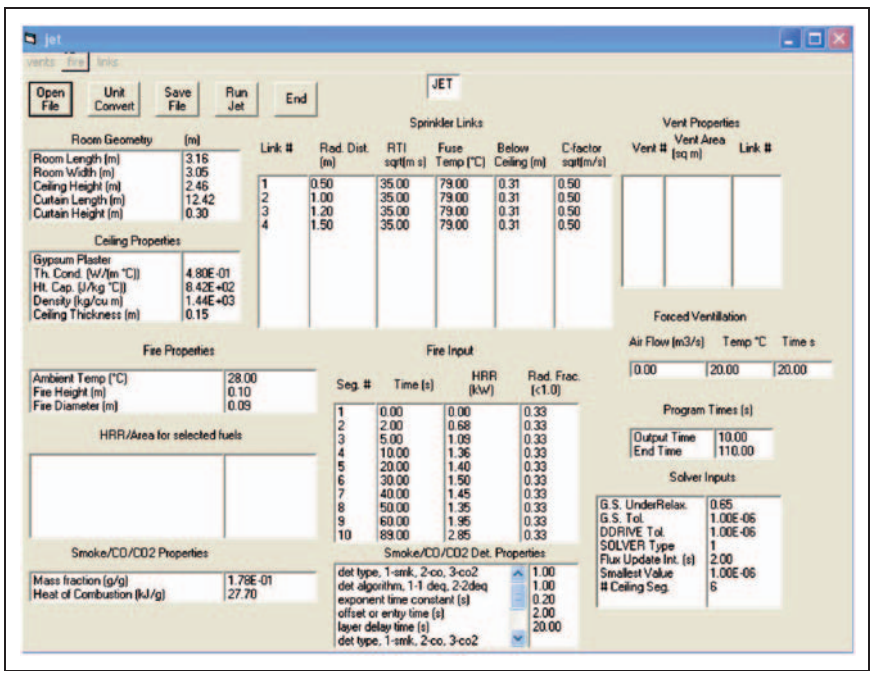

Figure 4. Example input file used to model Toluene.

account for the radiative fractions and smoke yields given in Table 1. The ceiling was approximated using the values for gypsum in order to simulate an insulating material.

The layer delay times were estimated by using the TT at 0.60 m from plume center and observing the time when the thermocouples at 0.24, 0.36, and 0.50 m began to respond to a changing temperature. Since these thermocouples were located where the layer would develop, their response would signal the beginning of the development of a layer. The layer response was estimated to the nearest 10 s.

The photoelectric smoke alarms used in these experiments were also used for the experiments reported in [6], which describes how the alarms were modified such that analog signals could be extracted from them. The alarms are residential alarms; all the alarms were manufactured by a single company. The photoelectric smoke alarms were calibrated in the FE/DE using a propene burner to produce smoke and a laser with a wavelength of 630 nm such that the extinction measured by the laser could be correlated with the photoelectric smoke alarm voltage. In general, the standard deviation for the extinction measurement was 1% and a sample curve fit is available in the Appendix. The typical range for the extinction measurements was $0.0\,m^{-1}$ to about $0.25\,m^{-1}$. For the toluene measurements, where the extinction was greater than $0.25\,m^{-1}$, the straight line fit to the calibration was extrapolated to larger values.

The lag and mixing times were measured using the FE/DE by covering the alarm with a can, setting the smoke flow to a constant value, and then removing the can, exposing the alarm to the smoke flow and measuring the response. Constant values for lag and mixing times of 2 and 0.2 s, respectively, were selected based on the FE/DE velocity dependent results. While the values of these constants are very important for predicting alarm activation times, this analysis was directed toward determining what information could be extracted from the alarm signals after the alarm had activated and hence these constants had negligible impact.

Results

Heptane

A 50 mL sample of heptane was ignited with the HRR, based on mass loss measurements, increasing from about 1.5 to 3.0 kW over a 500 s period (Figure 5). The vertical excess temperature distribution measured using the TT at 0.60 m from plume center 150 s after ignition provides a nice example of the ceiling jet (TT1, TT2, and TT3 located at 0.01, 0.03, and 0.06 m below the ceiling, respectively), the transition between ceiling jet and upper layer (TT4 at 0.12 m), and the roughly constant temperature of the upper layer (TT5, TT6, and TT7 located at 0.24, 0.36, and 0.50 m, respectively; Figure 6). The excess layer temperature averaged over the layer thermocouples are compared with the excess layer temperature

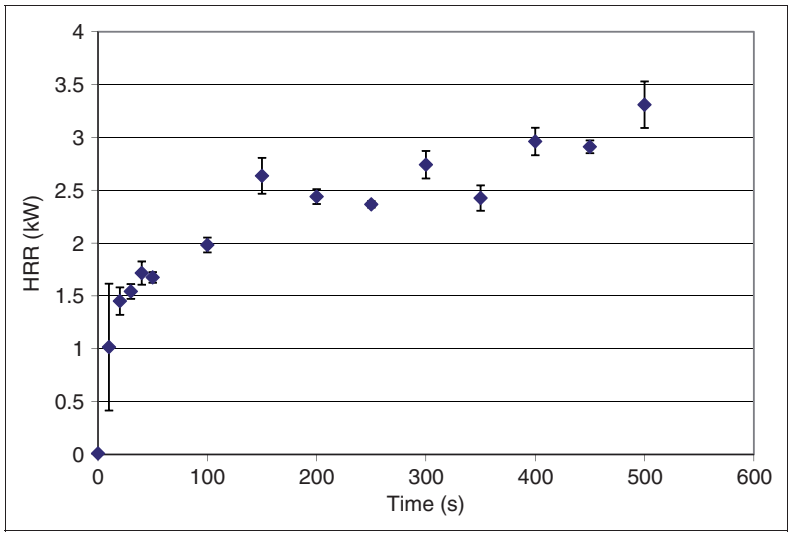

Figure 5. Heat release rate (HRR) for the heptane fire.
Note: The data were averaged over 5 data points (5 s) and are shown with the standard deviation associated with the averaging.

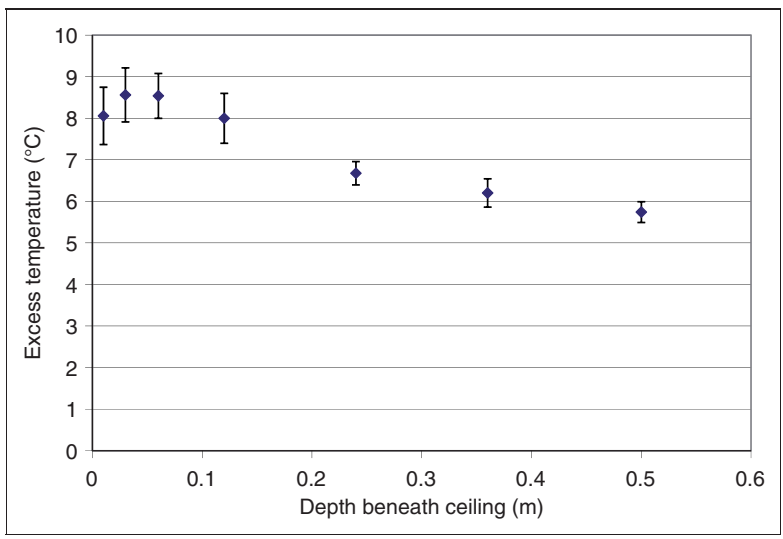

Figure 6. Vertical temperature profile for heptane at a radial distance of 0.60 m from fire center.
Note: Temperature points are located at 0.01, 0.03, 0.06, 0.12, 0.24, 0.36, and 0.50 m below the ceiling and the uncertainty interval represents one standard deviation over a 5 s interval.

calculated using JET. The measured excess layer temperature is 1–2°C higher than predicted by JET (Figure 7). JET over-predicts the ceiling jet temperature by about 2°C at a radius of 1.0 m from plume center (Figure 8). The thermocouples TC2 and TC7 were located at 1.0 m from plume center and make a 90° angle with a vertex at the plume centerline. The fact that these thermocouples do not agree suggests that the plume has moved off the geometric centerline. Using the excess temperature readings of the four thermocouples at 0.60 m (TC3, TC4, TC5, and TC6) the plume appears to be leaning toward TC4 (Figure 9) for the bulk of the experiment which would account for TC7 showing a lower excess temperature compared with TC2 and this movement may account for at least some of the temperature over-prediction.

Extinction coefficient measurements at 1.0 m from plume centerline are shown in Figure 10 for photoelectric smoke alarms and the laser. Also included is the prediction by JET for 1.0 m using smoke yields by Mulholland [18] and Tewarson [17]. The laser and photoelectric smoke alarms both depend on light scattering and absorption by the smoke particles. Using the Tewarson [17] smoke yield fraction, JET over-predicts the extinction deduced from the photoelectric smoke alarms. Using the Mulholland [18] smoke yield, JET predictions follow the extinction deduced by the photoelectric smoke alarms throughout the experiment. The laser measurement is also in agreement with the photoelectric smoke alarms until about 350 s.

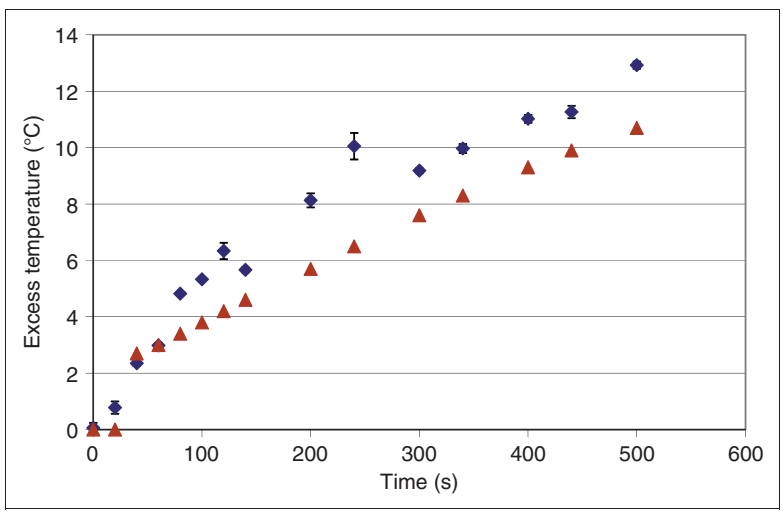

Figure 7. Average layer temperature for heptane (diamonds) compared with JET (triangles). Note: The average layer temperature and standard deviation uncertainty interval represent an average over the three tree thermocouples at 0.24, 0.36, and 0.50 m over a 5-point (s) interval.

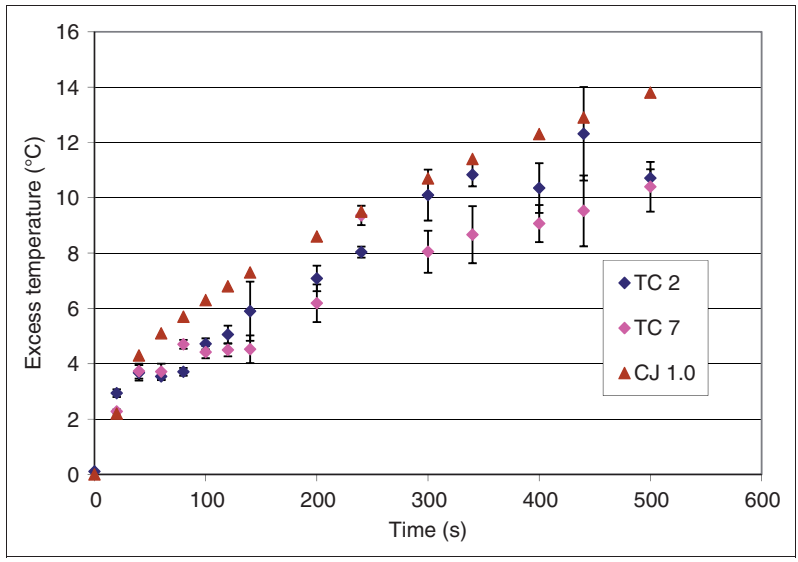

Figure 8. Comparison of measurements and JET for ceiling jet temperature at 1.0 m for heptane.
Note: The measurements are the purple diamond (TC2) and pink diamond (TC7) symbols with the triangles representing the predictions of JET. The standard deviation of the measurement represents an average over 5 points covering a time frame of 5 s.

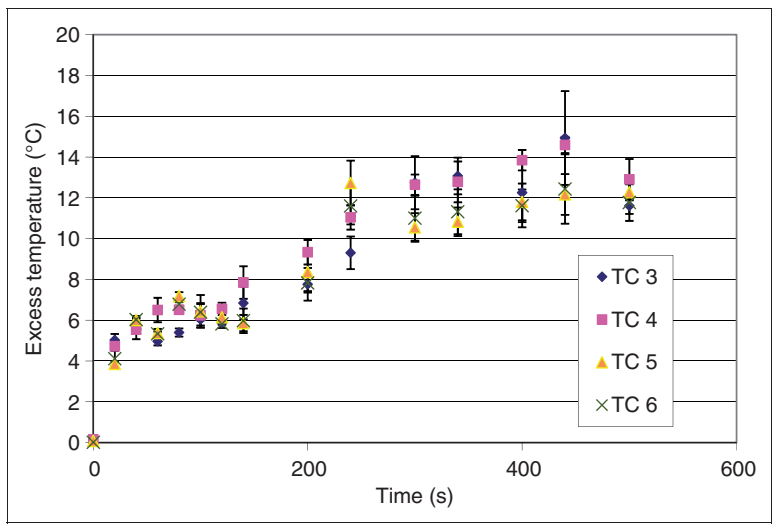

Figure 9. Temperature measurements at 0.6 m for heptane. A consistent lean toward TC4 is demonstrated over the entire experiment for the four thermocouples located 0.60 m from the plume centerline. The standard deviation of the measurement represents an average over 5 points covering a time frame of 5 s.

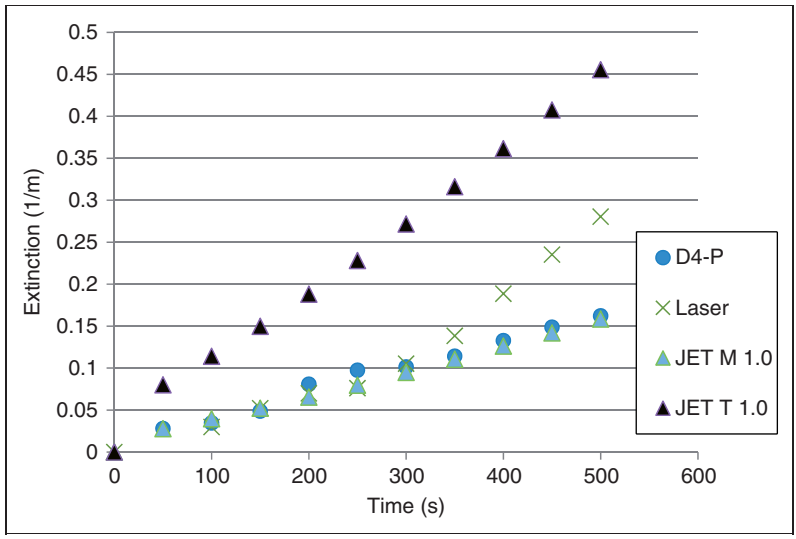

Figure 10. Comparison of photoelectric smoke alarms with the laser and predictions of JET using smoke fractions from Mulholland and Tewarson at 1.0 m for heptane.
Note: The dark blue circle is photoelectric smoke alarm A4P, the green X is the laser, the light blue triangle is JET using Mulholland's smoke fraction, and the brown triangle is JET using Tewarson's smoke fraction.

Toluene

A 10 mL sample of toluene was ignited with the HRR remaining constant at about 1.5 kW for the first 40 s and then increasing to almost 2.5 kW during the next 30 s (Figure 11). The excess layer temperature averaged over both the layer thermocouples and time is compared with the excess layer temperature calculated using JET with both the 0.33 and 0.60 radiative fractions. The measured excess layer temperature is within 1°C of the temperature predicted by JET for both values of the radiative fraction (Figure 12). JET over-predicts the ceiling jet temperature by at most 1°C at a radius of 1.0 m from plume center for most of the experiment using the 0.60 radiative fraction with the over-prediction reaching 2°C using the 0.33 radiative fraction value (Figure 13). The thermocouples TC2 and TC7 were located at 1.0 m from plume center and make a 90° angle with a vertex at the plume centerline. The fact that these thermocouples do not agree at all measurement points suggests that the plume was moving around the geometric centerline. Examination of the four thermocouples at 0.60 m (TC3, TC4, TC5, and TC6) show higher temperatures at TC4 and TC5 (Figure 14) suggesting that the plume centerline has moved in this direction.

Extinction coefficient measurements at 1.0 m from plume centerline are shown in Figure 15 for photoelectric smoke alarms and the laser. In general, the laser

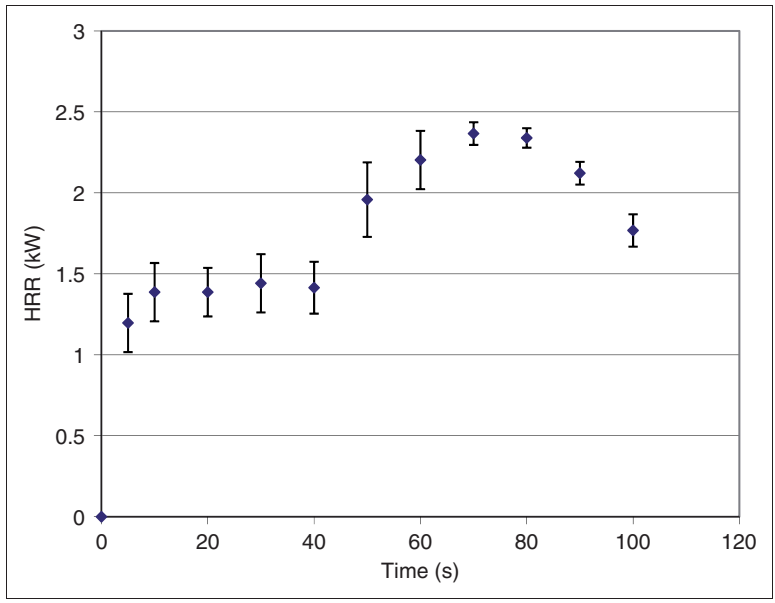

Figure 11. HRR for the toluene fire.
Note: The data were averaged over 5 data points (5 s) and are shown with the standard deviation associated with the averaging.

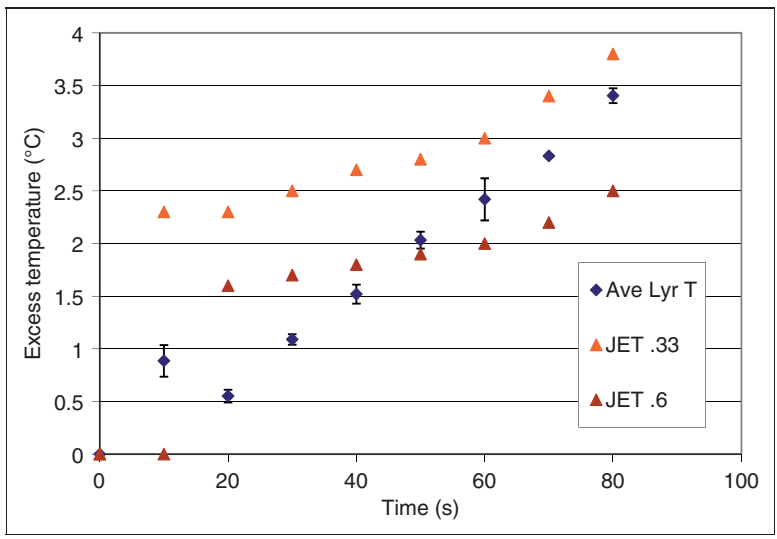

Figure 12. Average layer temperatures for toluene.
Note: The diamonds are the 5 s averaged temperature over the thermocouples at 0.24, 0.36, and 0.50 m located 0.60 m from plume center with the standard deviation shown. The orange and brown triangles are the predictions from JET for radiative fractions of 0.33 and 0.60, respectively.

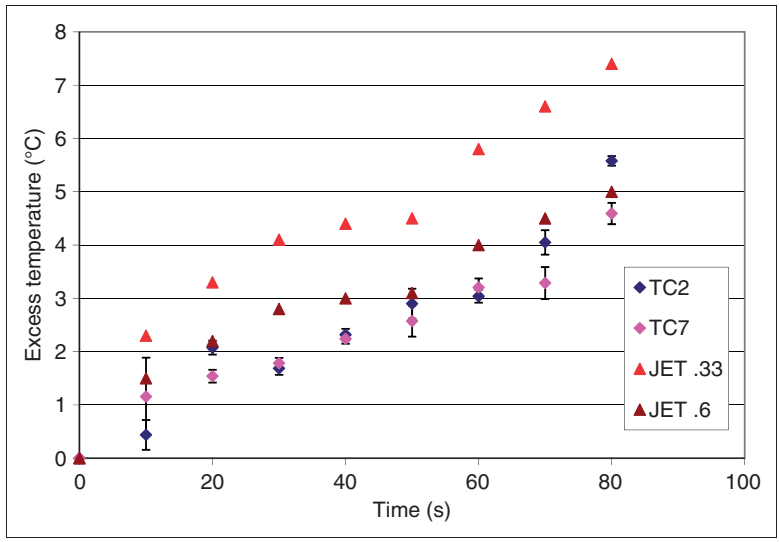

Figure 13. Comparison of ceiling jet measurements using TC2 and TC7 (purple and pink diamonds) and the predictions of JET (orange triangle for 0.33 radiative fraction and brown triangle for 0.60 radiative fraction) for toluene.
Note: The data were averaged over 5 data points (5 s) and are shown with the standard deviation associated with the averaging.

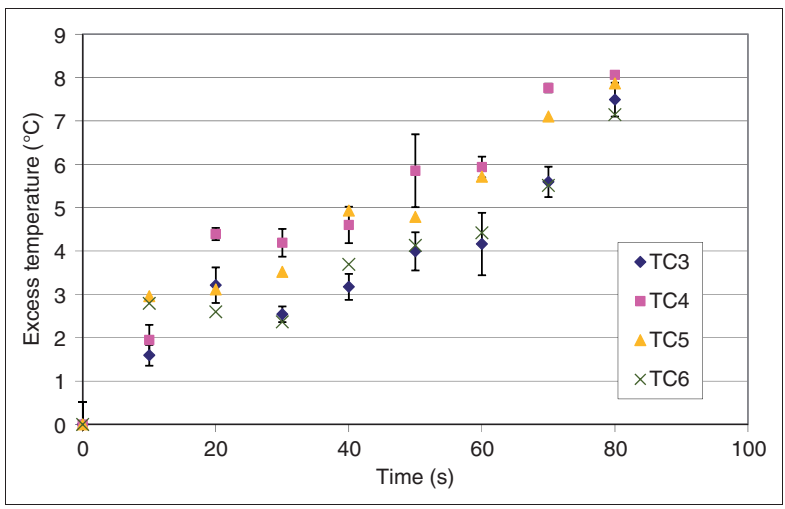

Figure 14. Temperature measurements at 0.6 m for toluene. A consistent plume lean toward TC4 is demonstrated starting at 20 s for the four thermocouples located 0.60 m from the plume centerline. The standard deviation of the measurement represents an average over 5 points covering a time frame of 5 s.

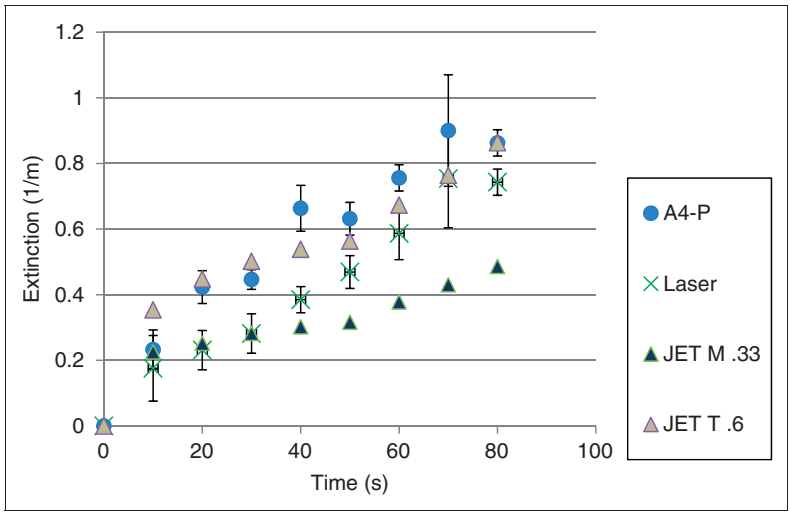

Figure 15. Comparison of photoelectric smoke (A4P blue circle) alarm, and laser (green X) with predictions of JET (dark blue triangle, Mulholland smoke yield and radiant fraction of 0.33 and light brown triangle, Tewarson smoke yield and radiant fraction of 0.6) for toluene.

exhibits the same slope as the photoelectric smoke alarm measurements but is about 0.2 m^{-1} smaller in value.

A comparison of the predictions of JET at 1.0 m from plume centerline using the smoke yields of Tewarson [17] and Mulholland [18], radiative fractions of 0.33 and 0.60 and the photoelectric smoke alarms and laser at the same distance is shown in Figure 15. Using Tewarson's [17] smoke yield, JET under-predicts the extinction deduced from the photoelectric smoke alarms. Using Mulholland's [18] smoke yield, JET follows the photoelectric smoke alarm over the measurement period. For times less than 50 s, the extinction measured by the laser is less than that deduced from the photoelectric smoke alarms but then starts to increase approaching the values obtained from the photoelectric smoke alarms. The different radiative fractions only impacted the model smoke predictions by about 10%.

Polymethyl-methacrylate

PMMA was ignited and the HRR increased to about 1.4 kW 1600 s after ignition (Figure 16). The excess layer temperature averaged over the layer thermocouples and in time is compared with the excess layer temperature calculated using JET. The measured excess layer temperature is within 0.5°C of the temperature predicted by JET (Figure 17). JET over-predicts the ceiling jet temperature by 1–2°C at a radius of 1.0 m from plume center for most of the experiment (Figure 18). The thermocouples TC2 and TC7 for Figure 18 were also located at 1.0 m from plume center and make a 90° angle with a vertex at the plume centerline (Figure 1). The fact that these thermocouples do not agree at all measurement points and that

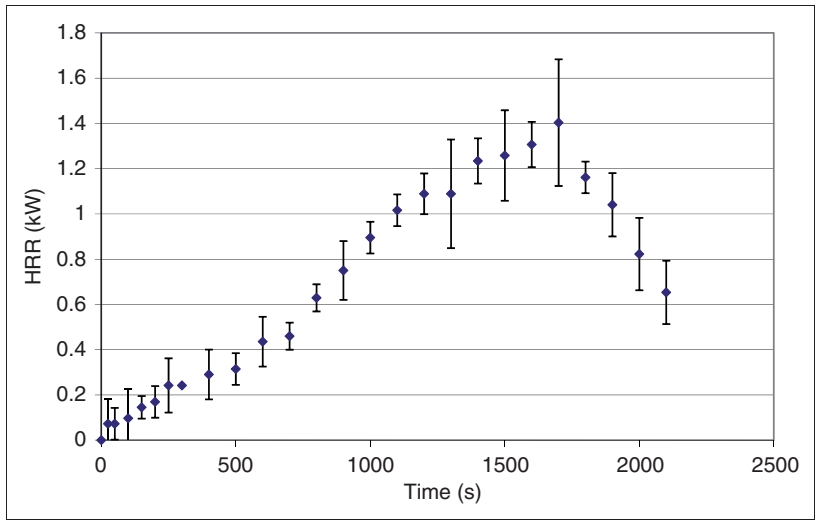

Figure 16. Heat release rate (HRR) for PMMA.

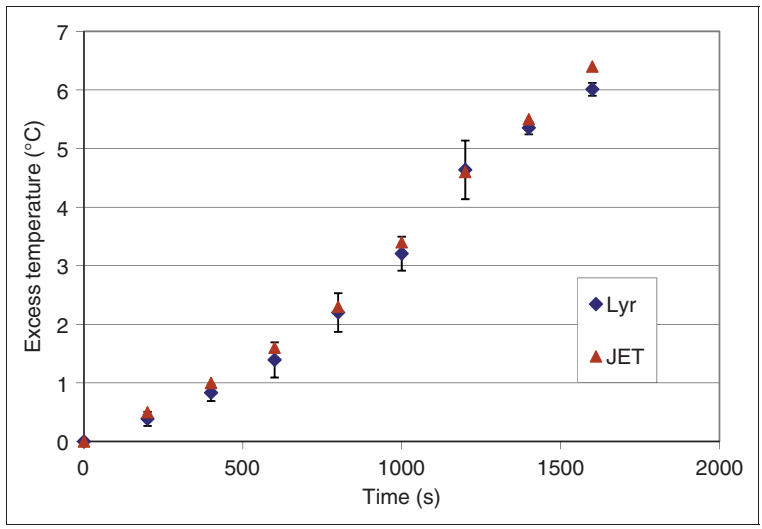

Figure 17. Average layer temperatures for PMMA.
Note: The diamonds are the 30 s averaged temperature over the thermocouples at 0.24, 0.36, and 0.50 m located 0.60 m from plume center with the standard deviation shown. The triangles are the predictions from JET.

the temperatures from these thermocouples are lower than the average layer temperature suggests that the plume has moved away from the geometric centerline. Examination of the four thermocouples at 0.60 m (TC3, TC4, TC5, and TC6) show higher temperatures at TC4 (Figure 19) suggesting that the plume centerline has

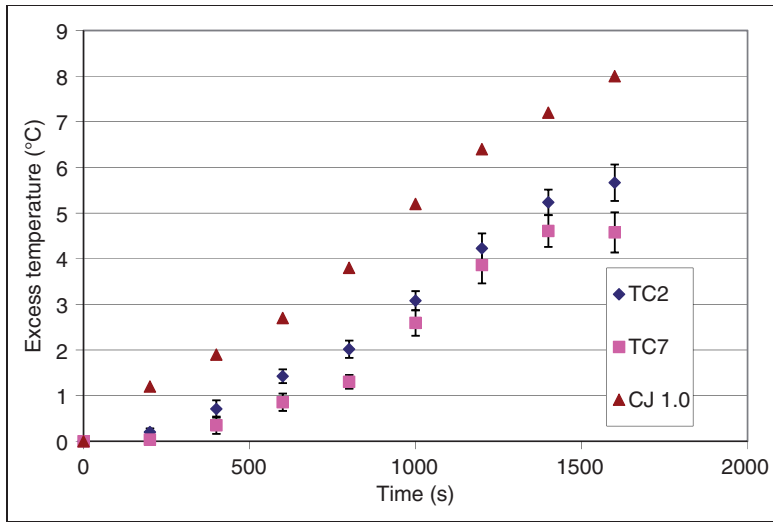

Figure 18. Comparison of ceiling jet measurements using TC2 and TC7 (purple diamond and pink square) with the predictions of JET (brown triangle) for PMMA.
Note: The data were averaged over 30 data points (30 s) and are shown with the standard deviation associated with the averaging.

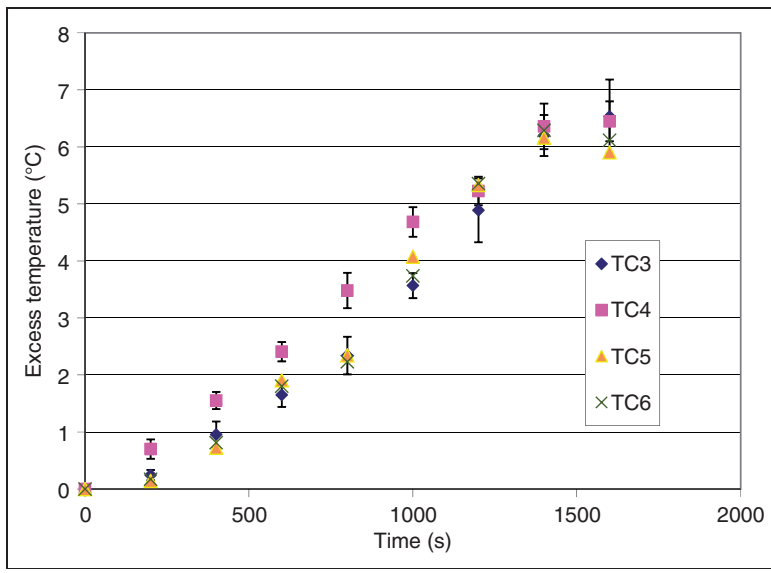

Figure 19. Temperature measurements at 0.6 m for PMMA. A consistent lean toward TC4 is demonstrated for the first 1000 s for the four thermocouples located 0.60 m from the plume centerline. The standard deviation of the measurement represents an average over 30 points covering a time frame of 30 s.

moved in this direction although between 1200 and 1600 s, the four thermocouples are in agreement.

PMMA smoke extinction coefficient values at 0.5 and 1.0 m from the plume centerline are shown in Figure 20 for photoelectric smoke alarms and the laser as well as the predictions by JET for 0.5 and 1.0 m using the PMMA smoke yield from Tewarson [17]. The photoelectric smoke alarms and the laser require about 1000 s after ignition before any response occurs. A comparison of the predictions of JET at 0.5 and 1.0 m from plume centerline and the photoelectric smoke alarm at 1.0 m shows poor agreement, with JET over-predicting the extinction.

Discussion

The three fuels used in this study of detector response and modeling for flaming fires provide an excellent comparison set as each fire produced a unique detector response to the produced smoke. Based on a previous study by Mulholland [21], it is expected that photoelectric smoke alarms will respond quickly to fires, such as those that smolder smoldering and produce large smoke particles. The color of the smoke is also important for devices that depend on scattering for a signal such as the photoelectric smoke alarms examined here. This is quite evident for the burning

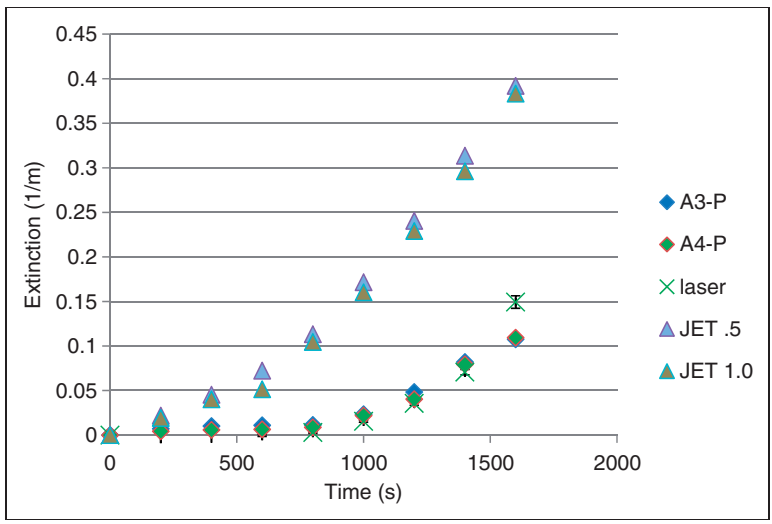

Figure 20. Comparison of photoelectric smoke alarm and laser measurements with the predictions of JET for PMMA.
Note: The dark blue and green diamonds are the photoelectric smoke alarm measurements at 0.5 and 1.0 m from plume center, the dark green X is the laser measurement at 1.0 m and the light blue and brown triangles are the predictions of JET at 0.5 and 1.0 m. The measurement and standard deviation represent an average over 10 points covering a time frame of 10 s.

black PMMA as neither the photoelectric smoke alarm nor the laser provided a timely response to this fire.

The predictions of JET were quite instructive and demonstrated the need to understand the basis of smoke yields in the literature. Using the smoke yields published by Mulholland [18], JET predicted the measured extinction determined from the laser and the photoelectric smoke alarm for heptane. Using the smoke yields of Tewarson [17], JET predicted the measured extinction determined from the photoelectric smoke alarm for toluene. Only a smoke yield fraction from Tewarson [17] was available for PMMA and JET over-predicted the extinction measured by the photoelectric smoke alarms.

Limitations

When comparing a computer model with experiments, both the measurement uncertainties of the experiment and the uncertainty of the input values used by the model must be considered (see Ref. [12] for examples of this comparison). For this set of experiments, the measurements to be considered include the temperature measurements by the thermocouples, the mass loss measurement using a load cell, the photoelectric smoke alarm measurements, and the laser measurement. An array of thermocouples will provide absolute temperature measurements that will vary by roughly 1°C from thermocouple to thermocouple. Since excess temperature rather than absolute temperature is reported, this variation will be eliminated. The temperatures reported represent averages over time with the uncertainty interval providing a measure of the variation in the average temperature. A second uncertainty is the issue of the plume moving off the plume centerline. This effect makes it difficult to determine the radial trends with any precision. For these experiments, the thermocouple distribution near the plume center was dense enough to determine the direction of the plume lean but not the radial location of plume center in time.

The TT was used to measure the vertical temperature profile of the ceiling jet at 0.6 m from the fire centerline. The measured excess temperature of the ceiling jet was relatively constant for the three measurements that extended to 0.06 m beneath the ceiling which supports the assumption that the photoelectric smoke alarms as well as the laser were sampling the ceiling jet.

Uncertainty for the laser measurement was primarily based on the fluctuation of the fire and is represented by the uncertainty interval presented in the graphs. A second issue with the laser is its sensitivity to temperature. In an earlier experiment testing JET, the laser used to measure extinction was not cooled and deviated quickly from the extinction values obtained from the photoelectric smoke alarms. The diode laser and diode detector used for these experiments were air cooled but still exhibited temperature driven deviations from the photoelectric smoke alarms at about 350 s when the temperature was 38°C, for the higher temperature heptane experiments.

The user inputs for the model include room dimensions, detector locations, ambient temperature, fire diameter and height of ceiling above the fire, HRR, radiative fraction, chemical heat of combustion, and smoke yield. For these experiments, the room dimensions, detector locations, height of the ceiling above the fire and ambient temperature are all known with an uncertainty of less than 1%. A fixed fire diameter either equal to the size of the dish containing the liquid fuel or the size of the PMMA block was used for this modeling.

Of the remaining variables, HRR, radiative fraction, chemical heat of combustion, and smoke yield, the HRR is calculated by multiplying the chemical heat of combustion by the mass loss which is measured by the load cell. As long as the fire is well ventilated, as it was for these experiments, the calculated HRR should have an error of less than 5% based on the load cell measurement. Additional error is dependent on the accuracy of the actual chemical heat of combustion. Typically, uncertainties for this value are not readily available in the literature. The radiative fraction as a function of fire size has only been determined for a few special cases [21]. For the comparisons here, the radiative fraction should be close to the value in the literature as the fires used in these experiments are small and will not have the absorptive issues found in larger fires [22]. In the case of the toluene experiment, the large difference in radiative fractions had only a small impact on the smoke algorithms. While the ceiling jet temperature comparison favored the larger radiative fraction, the only sensible approach is to suggest that the radiative fraction of toluene be measured again to sort out this uncertainty. Of the inputs for JET, the major issue is the smoke yield. In the analysis for heptane, the smoke yield determined by two different researchers differed by a factor of 2.9. A number of issues could explain this difference including differing fire sizes and measurement techniques.

The final parameter to consider in understanding the uncertainty associated with this comparison is not an input parameter to the model but is the factor $8.7 \pm 1.1\,\mathrm{m^2\,g^{-1}}$ that is used to convert the calculated smoke concentration to an extinction value. The uncertainty interval represents the extended uncertainty that encompasses 95% of the values surveyed in all studies. The uncertainty in this factor is just under $\pm 13\%$ and represents the largest uncertainty after the smoke yield for toluene and heptane and the radiative fraction for toluene. It should be noted that the uncertainty intervals used in this article represent $\pm\sigma$ and not $\pm 2\sigma$ as is usually quoted for this value.

Conclusion

Modeling the output of photoelectric smoke alarms using JET has met with limited success in that JET was able to predict the alarm signals using different smoke yields for heptane and toluene but was unable to follow the signals for black PMMA. The fact that different smoke yields had to be used to follow the

photoelectric smoke alarm signal outputs for heptane and toluene is disturbing. For successful use of this model for photoelectric smoke alarms, there must be an improved understanding of how smoke yield for materials currently tabulated in the literature correlates with the response of these types of detectors. There also must be an understanding of how fire size impacts smoke yield and alarm response. The black PMMA result was expected and demonstrates the need for understanding the impact of materials on smoke alarm response.

The uncertainty in radiative fraction for toluene proved to be of minor importance for smoke prediction but if temperature prediction is required, this parameter must be better understood.

References

1. Alpert RL. Calculation of response time of ceiling-mounted fire detectors. *Fire Technology* 1972; Vol. 8(3): 181–195.
2. Evans DD and Stroup DW. Methods to calculate the response time of heat and smoke detectors installed below large unobstructed ceilings. *Fire Technology* 1985; Vol. 22(1): 54–63.
3. Heskestad G and Delichatsios MA. *Environments of fire detectors phase 1; effects of fire size, ceiling height and material, volume II – analysis*. Technical Report Serial No. 22427, RC 77-T-11. Norwood, MA: Factory Mutual Research Corporation, 1977, pp.1–100.
4. Schifiliti RP. Fire detection modeling – the research application gap. In: *AUBE '01, 12th International conference on automatic fire detection*. Gaithersburg, MD USA, National Institute of Standards and Technology, 2001.
5. Bukowski RW and Averill JD. Methods for predicting smoke detector activation. In: *Fire Suppression and Detection Research Application Symposium, Research and Practice: Bridging the Gap*. National Fire Protection Research Foundation, Quincy, MA, 1998.
6. Bukowski RW, Peacock RD, Averill JD, Cleary TG, Bryner NP, Walton WD, et al. *Performance of home smoke alarms: analysis of the response of several available technologies in residential fire settings*. NIST TN 1455-1. Gaithersburg, MD: National Institute of Standards and Technology, 2007, pp.1–396.
7. Davis WD and Notarianni KA. *NASA fire detector study*. NISTIR 5798. Gaithersburg, MD USA: National Institute of Standards and Technology, 1996, pp.1–33.
8. Klote J, Davis WD, Forney GP and Bukowski R. *Field modeling: simulating the effects of HVAC induced air flow from various diffusers and returns on detector response*. Year Four Report. National Fire Protection Research Foundation, Quincy, MA, 1998.
9. Alpert RL. Turbulent ceiling-jet induced by large-scale fires. *Combustion Science and Technology* 1975; Vol. 11: 197–213.
10. Yamauchi Y. *Prediction of response time of smoke detectors in enclosure fires*. NBSIR88-3707. Gaithersburg, MD: National Institute of Standards and Technology, 1988, pp.1–46.

11. Davis WD. *Zone fire model jet: a model for the prediction of detector activation and gas temperature in the presence of a smoke layer*. NISTIR 6324. Gaithersburg, MD: National Institute of Standards and Technology, 1991, pp.1–55.
12. Davis WD, Cleary TG, Donnelly MK and Hellerman SD. *Predicting smoke and carbon monoxide detector response in the ceiling jet in the presence of a smoke layer*. NISTIR 6976. Gaithersburg, MD: National Institute of Standards and Technology, 2003, pp.1–35.
13. Cleary TG, Chernovsky A, Grosshandler WL and Anderson M. Particulate entry lag in spot-type smoke detectors. In: Curtat M (ed.) *Fire Safety Science – Proceedings of the Sixth International Symposium*. London: International Association for Fire Safety Science (IAFSS), 2000.
14. Grosshandler W. Toward the development of a universal fire emulator-detector evaluator. *Fire Safety Journal* 1997; Vol. 29: 113–128.
15. Mulholland GW and Croarkin C. Specific extinction coefficient of flame generated smoke. *Fire and Materials* 2000; Vol. 24: 227–230.
16. Mun JZ, Choi Y, Mulholland GW and Gritzo LA. Soot scattering measurements in the visible and near-infrared spectrum. *Proceedings of the Combustion Institute* 2000; Vol. 28: 439–436.
17. Tewarson A. Generation of heat and chemical compounds in fires. In: DiNenno PJ, Drysdale D, Beyler CL, Walton WD, Custer RLP, Hall Jr JR, et al. *The SFPE handbook of fire protection engineering*. 3rd ed. Quincy, MA: National Fire Protection Association, 2002, pp.3-82–3-161.
18. Mulholland GW, Johnsson EL, Fernandez MG and Shear DA. Design and testing of a new smoke concentration meter. *Fire and Materials* 2000; Vol. 24: 231–243.
19. Gore JP, Klassen M, Hamins A and Kashiwagi T. *Fire safety science – proceedings of the third international symposium*. London: Elsevier, 1991.
20. Wade RW, Sivathanu YR and Gore JP. Soot volume fraction and temperature properties of high liquid loading spray flames. In: *Proceedings: Combustion Fundamentals and Applications*. Joint Meeting of the Central and Western States Sections, Mexican National Section and American Flame Research Committee, Pittsburg, PA, The Combustion Institute, 1995.
21. Mulholland GW. Smoke production and properties. In: DiNenno PJ, Drysdale D, Beyler CL, Walton WD, Custer RLP, Hall Jr JR, et al. *The SFPE handbook of fire protection engineering*, 3rd ed. Quincy, MA: National Fire Protection Association, 2002, pp.2-258–2-268.
22. Yang JC, Hamins A and Kashiwagi T. Estimate of the effect of scale on radiative heat loss fraction and combustion efficiency. *Combustion Science and Technology* 1994; Vol. 96: 183–188.

Appendix

Figure A1 provides an example of the calibration curves used to convert the smoke alarm signals to extinction coefficients for each photoelectric smoke alarm. Each alarm was placed in the FE/DE and subjected to varying levels of smoke using a propene calibration fire. The extinction produced at each smoke level was measured by a laser operating at a wavelength of 630 nm. Table A1 provides a summary of the curve fits for the equations.

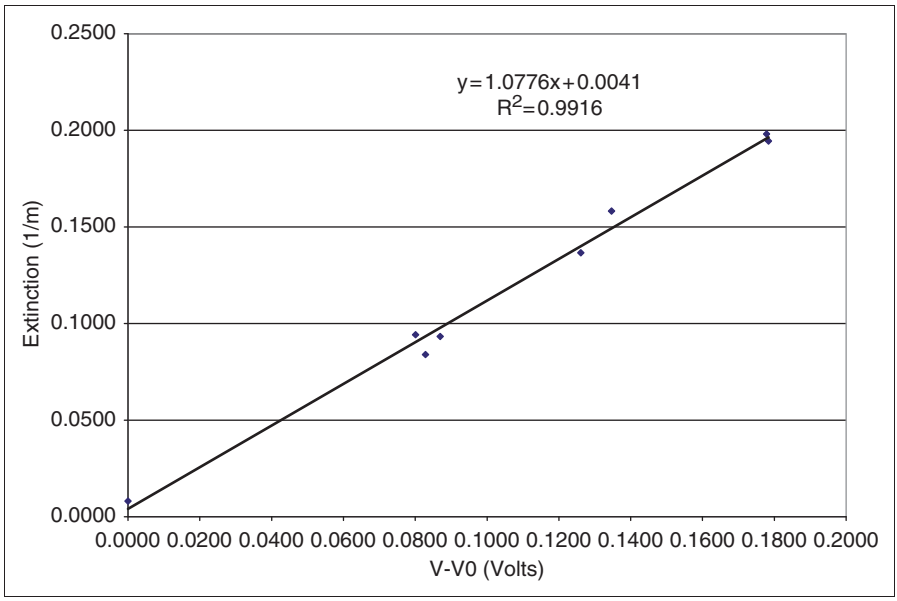

Figure A1. Photoelectric smoke Alarm A1P calibration with propene in the NIST FE/DE.

Table A1. Calibration equations for the photoelectric smoke alarms.

Alarm	Equation	R^2
A1P	$Y = 1.0776X + 0.0041$	0.9916
A2P	$Y = 0.9365X + 0.0014$	0.9631
A3P	$Y = 0.8649X + 0.0103$	0.9555
A4P	$Y = 1.4426X - 0.0094$	0.9633
A5P	$Y = 1.2229X - 0.0017$	0.9931

Y is the extinction coefficient (m^{-1}), X the detector voltage (V), and R the Pearson value for the fit.